

QUT Digital Repository:
<http://eprints.qut.edu.au/>



Adam, Clayton J. and Askin, Geoffrey N. (2009) *Lateral bone density variations in the scoliotic spine*. BONE, 45(4). pp. 799-807.

© Copyright 2009 Elsevier Ltd

1 **Lateral bone density variations in the scoliotic spine**

2

3 Clayton J Adam¹, PhD; Geoffrey N Askin², FRACS

4

5 1. Paediatric Spine Research Group, Institute of Health and Biomedical Innovation, Queensland

6 University of Technology, Brisbane, Australia.

7 2. Mater Health Services Brisbane Ltd, Brisbane, Australia.

8

9

10 **Corresponding Author**

11 Dr Clayton Adam

12 Paediatric Spine Research Group

13 Level 2, Mater Children's Hospital

14 Raymond Terrace, South Brisbane Q4101, Australia

15 Phone: +61 7 3163 6162

16 Mobile: 0405 148 686

17 Fax: +61 7 3163 1744

18 Email: c.adam@qut.edu.au

1 **Abstract**

2 Adolescent Idiopathic Scoliosis (AIS) is the most common deformity of the spine, affecting 2-4%
3 of the population. Previous studies have shown that the vertebrae in scoliotic spines undergo
4 abnormal shape changes, however there has been little exploration of how scoliosis affects bone
5 density distribution within the vertebrae.

6

7 In this study, existing CT scans of 53 female idiopathic scoliosis patients with right-sided main
8 thoracic curves were used to measure the lateral (right to left) bone density profile at mid-height
9 through each vertebral body. Five key bone density profile measures were identified from each
10 normalised bone density distribution, and multiple regression analysis was performed to explore
11 the relationship between bone density distribution and patient demographics (age, height, weight,
12 body mass index (BMI), skeletal maturity, time since Menarche, vertebral level, and scoliosis
13 curve severity).

14

15 Results showed a marked convex/concave asymmetry in bone density for vertebral levels at or
16 near the apex of the scoliotic curve. At the apical vertebra, mean bone density at the left side
17 (concave) cortical shell was 23.5% higher than for the right (convex) cortical shell, and cancellous
18 bone density along the central 60% of the lateral path from convex to concave increased by
19 13.8%. The centre of mass of the bone density profile at the thoracic curve apex was located
20 53.8% of the distance along the lateral path, indicating a shift of nearly 4% toward the concavity
21 of the deformity. These lateral bone density gradients tapered off when moving away from the
22 apical vertebra. Multi-linear regressions showed that the right cortical shell peak bone density is
23 significantly correlated with skeletal maturity, with each Risser increment corresponding to an
24 increase in mineral equivalent bone density of 4-5%. There were also statistically significant
25 relationships between patient height, weight and BMI, and the gradient of cancellous bone density

1 along the central 60% of the lateral path. Bone density gradient is positively correlated with
2 weight, and negatively correlated with height and BMI, such that at the apical vertebra, a unit
3 decrease in BMI corresponds to an almost 100% increase in bone density gradient.

4
5

1 **Introduction**

2 Adolescent Idiopathic Scoliosis (AIS) is the most common deformity of the spine, affecting 2-4%
3 of the population. Previous studies have shown that the vertebrae in scoliotic spines undergo
4 abnormal morphological changes including wedging in the coronal plane [1-9], pedicle asymmetry
5 [10-16], spinous process asymmetry [17-21], and intravertebral torsion between the superior and
6 inferior vertebral endplates [22,23].

7

8 While vertebral shape is clearly important in the biomechanics of spinal deformity and its surgical
9 treatment, the bone density distribution *within* the vertebrae is equally important for three reasons.
10 Firstly, asymmetries in bone density are an adaptive response to asymmetrical loading, so the
11 degree of asymmetry in bone density is an indicator of the degree of asymmetrical loading to
12 which the scoliotic spine is subjected. Secondly, because bone density governs vertebral stiffness,
13 lateral variations in bone density are indicative of asymmetries in axial stiffness from one side of
14 the vertebrae to another, which has important implications for studies of mechanically-modulated
15 bone growth in scoliosis. Thirdly, vertebral bone density is the most important determinant of
16 pullout strength of implants used in anterior scoliosis surgery [24]. Implant pullout rates of around
17 5% have been reported following anterior scoliosis surgery [25].

18

19 Most studies of bone density in adolescent scoliosis have focused on overall reductions in bone
20 mineral density (BMD) compared to normal controls [26-29]. To our knowledge, the only current
21 studies of bone density *distribution* in AIS are those of Périé *et al* [30-32], who found that the
22 centre of mass in lumbar scoliotic vertebrae migrated toward the concavity of the scoliotic curve,
23 implying higher bone density on the concave side than on the convex side¹. While Périé's studies

¹ Routh *et al* [33] found the same pattern in postmenopausal women with adult degenerative scoliosis

1 highlight an important aspect of the deformity, the eleven girls involved all had mild scoliotic
2 curves, and the bone density migration was only measured for one vertebral level in each patient.

3
4 With these considerations in mind, the aim of this paper was to quantify how bone density varies
5 laterally in the vertebrae of scoliotic spines using computed tomography (CT) images of a larger
6 group of AIS patients with more severe deformities, and to explore how the lateral bone density
7 profile is affected by patient height, weight, body mass index, skeletal maturity, vertebral level,
8 and scoliosis curve severity.

9

10 **Materials and Methods**

11

12 *CT scans*

13 A series of existing pre-operative CT scans which were previously performed for surgical
14 planning purposes at the Mater Children's Hospital in Brisbane, Australia between 2002 and 2008,
15 were retrieved from archives. A single low-dose CT scan is part of the pre-operative clinical
16 assessment process for patients scheduled to undergo endoscopic anterior instrumented scoliosis
17 correction, since pre-operative CT has been shown to allow safer screw sizing and positioning in
18 endoscopic procedures [34]. Only scans of females with right-sided thoracic curves were
19 retrieved, as this is the most common gender and curve type among AIS patients.

20

21 Four different CT scanners were used over the six year period from which the scans were
22 retrieved; (i) a 4-slice Toshiba Aquilion (Toshiba Medical Systems, Tokyo, Japan) with 100kV
23 50mA source and 3mm raw image thickness, (ii) a 64-slice Philips Brilliance (Philips Healthcare,
24 Andover, USA) with 120kV 50mA source and 2mm raw image thickness, (iii) a 64 slice GE
25 Lightspeed Plus (GE Healthcare, Chalfont St Giles, UK) with 100kV 50mA source and 2.5mm

1 raw image thickness, and (iv) a 64 slice GE Lightspeed VCT (GE Healthcare, Chalfont St Giles,
2 UK) with 100kV 50mA source and 2.5mm raw image thickness. The scan coverage in each case
3 was from vertebral levels C7 to S1. Dose reports were commissioned for all four scanners, and the
4 highest estimated radiation dose of 3.7mSv occurred with the oldest scanner (Toshiba Aquilion),
5 with uncertainties due to the dose model in the order of $\pm 20\%$ (*Schick D, Computed Tomography*
6 *radiation doses for paediatric scoliosis scans. Internal report commissioned by Paediatric Spine*
7 *Research Group from Queensland Health Biomedical Technology Services, 2004*). By
8 comparison, annual background radiation in Queensland is approximately 2.0mSv per annum.
9 Estimated doses for the newer 64 slice scanners were substantially lower (in the order of 2mSv).
10 Pixel dimensions in the reconstructed axial CT slices varied from 0.53-0.76mm.

11

12 *Image processing*

13 Following retrieval of the CT scans, the ImageJ software (version 1.38x, National Institutes of
14 Health, USA) was used to generate reformatted two-dimensional images through the mid-height
15 of each vertebral body, parallel to the plane of the vertebral endplates as shown in Figure 1. To
16 assess lateral variations in bone density through each vertebral body, an antero-posterior line was
17 drawn joining the most anterior edge of the neural canal with the most anterior edge of the
18 vertebral body. A second line, perpendicular to the first, was then drawn through the vertebral
19 body at the point where its width was a maximum. CT values (Hounsfield Units, HU) were
20 extracted for each pixel along this lateral line. The position of the antero-posterior and lateral
21 (right to left) lines is shown in Figure 2 (marked AP and Lat respectively). The CT value profile
22 along the lateral line was measured for each vertebral body between T1 and L5 (inclusive). To
23 allow comparison between vertebrae of differing widths, distance along the lateral path was
24 normalized in each case, with 0 corresponding to the right-most edge and 1 to the leftmost edge of
25 the lateral path.

1
2
3
4
5
6
7
8
9
10
11
12
13
14
15
16
17
18
19
20
21
22
23
24
25

Bone density measurements

In order to convert the CT values in Hounsfield units from the four scanners to a quantitative bone mineral density measurement, a Calcium Chloride (CaCl_2) phantom containing 6.8mmol of Calcium ions per 10mL of solution was imaged in each scanner using the scan parameters described above. Accordingly, the bone density results below are expressed as equivalent mineral density in milligrams of Calcium per cubic centimetre ($\text{mg.cm}^{-3} \text{Ca}$). The lateral bone density profiles for each vertebra were then used to calculate the following five bone density parameters (shown schematically in Figure 3). Each parameter was given a three letter abbreviation;

- RSP – **R**ight **c**ortical **s**hell **p**eak bone density ($\text{mg.cm}^{-3} \text{Ca}$)
- LSP – **L**eft **c**ortical **s**hell **p**eak bone density ($\text{mg.cm}^{-3} \text{Ca}$)
- MCP - **M**ean bone density along the **c**entral 60% of the lateral **p**ath ($\text{mg.cm}^{-3} \text{Ca}$)
- GCP – **G**radient of bone density along the **c**entral 60% of the lateral **p**ath ($\text{mg.cm}^{-3} \text{Ca}$)
- COM – **C**entre **o**f **M**ass location of the bone density distribution along the lateral path (%)

Note that because all patients had right thoracic major curves, RSP and LSP refer to the convex and concave sides of the major curve respectively (see Figure 1). For parameters MCP and GCP, the central 60% of total vertebral width was chosen to provide a representative section of the cancellous bone centrum, while avoiding the two cortical peaks. Note also that because the distance along the lateral path is normalized by the total vertebral width, the units of bone density gradient (GCP) are the same as the units for mineral equivalent bone density. The location of the Centre of Mass (COM) along the lateral bone density profile at each vertebral level was defined as:

1
$$COM = \frac{\sum \rho_i x_i}{\sum \rho_i} \quad [1]$$

2

3 where ρ_i is the mineral equivalent bone density ($\text{mg}\cdot\text{cm}^{-3}$ Ca) of pixel i at normalized distance x_i
4 along the lateral path ($0 < x_i < 1$).

5

6 *Statistical analysis*

7 The individual bone density profiles for each patient were then pooled to obtain the 10th, 50th
8 (median) and 90th percentile bone density profiles at each vertebral level from T1 to L5, as well as
9 the mean, median, range and standard deviation of each of the five parameters (RSP, LSP, MCP,
10 GCP, COM) defined above.

11

12 To account for the differences in scoliotic curve apex location between patients, lateral bone
13 density profiles were also determined for the seven vertebral levels $A+3, A+2, A+1, A, A-1, A-2, A-$
14 3 , where A represents the apical vertebral level of the major scoliotic curve in the coronal plane
15 (defined as the most laterally deviated vertebra on a coronal plane radiograph), and \pm represent
16 the number of levels relative to the apex in the inferior and superior directions respectively (eg $A-1$
17 is the level immediately superior to the apex). If the apical level was a disc, then by convention the
18 superior adjacent vertebra was defined as the apical vertebral level. Seven vertebral levels
19 centered on the apex of the deformity were chosen because this range approximately spans the
20 main thoracic curve.

21

22 To assess the association between vertebral bone density profiles and key clinical measures in AIS
23 patients, multi-linear regressions were performed for each of the five bone density parameters (as
24 the dependent variable) using the following nine clinical measures as the independent variables:

- 1 1. Age (years)
- 2 2. Height (cm)
- 3 3. Weight (kg)
- 4 4. Body Mass Index (BMI, $\text{kg}\cdot\text{m}^{-2}$)²
- 5 5. Risser sign³
- 6 6. Time since Menarche (months)⁴
- 7 7. Cobb angle of the major curve (degrees)⁵
- 8 8. Upper vertebral level of the major curve
- 9 9. Lower vertebral level of the major curve

10

11 Separate multi-linear regressions were performed for each vertebral level (T1 to L5) and also for
12 vertebral levels expressed relative to the apex ($A-3$ to $A+3$). Statistical analyses were performed
13 using SPSS version 16.0 (Chicago, USA).

14

15 **Results**

16 Fifty-three patients were included in the study, for a total of $53 \times 17 = 901$ vertebral bodies. By
17 selection, all patients were female adolescent idiopathic scoliosis patients with right thoracic major
18 curves. Demographic and scoliosis curve details for the group are summarized in Table 1. Further
19 details for each individual patient (age, height, weight, BMI, Risser sign, major curve levels, and
20 major Cobb angle) are given in Appendix 1. All curves were classified as Type 1 according to the
21 Lenke classification [35], with 34 type 1A, 12 type 1B, and 7 type 1C. The skeletal maturity

² Body Mass Index is defined as weight (in kilograms) divided by the square of height (in meters)

³ A measure of skeletal maturity defined by the amount of calcification of the iliac apophysis, ranging from 0 (skeletally immature, no fusion) to 5 (iliac apophysis fused to iliac crest after complete ossification).

⁴ Months since first menstruation. For cases where Menarche was more than 5 years ago, this variable was set to 60 months. For pre-Menarche subjects, the value was 0.

⁵ Cobb angle is a measure of the severity of a scoliotic curve, defined as the angle (in degrees) formed between the superior-most and inferior-most endplates (respectively) of the upper and lower end vertebrae of a scoliotic curve (refer Fig 1).

1 (Risser sign) of patients in the group at the time of the CT scan varied across the full range of
2 possible Risser values (0 to 5).

3

4 Figure 4 shows the distribution (10th, 50th and 90th percentile) of mineral equivalent bone density
5 profiles for each of the 17 vertebral levels in the thoracolumbar spine. Figures 5, 6 and 7 show the
6 mean values for the bone density profile parameters MCP, GCP, and COM respectively versus
7 vertebral level.

8

9 Table 2 provides full summary statistics on each of the five bone density profile measures (RSP,
10 LSP, MCP, GCP, COM) defined earlier. Table 3 gives summary statistics of the same five
11 measures for vertebral levels relative to the apical vertebral level (*A*) of each patient's major
12 curve, from *A*-3 to *A*+3.

13

14 Table 4 lists any statistically significant independent variables in the multi-linear regressions. For
15 example, the regression for Centre of Mass (COM) of the bone density distribution at T7 was
16 significantly correlated with both Risser sign and Cobb angle of the major curve. Empty cells in
17 Table 4 indicate that none of the terms in that regression equation were statistically significant.
18 For statistically significant terms, the corresponding coefficient in the regression equation is given
19 in brackets.

20

21 **Discussion**

22 Although the etiology of AIS is still unclear, it is generally agreed that progression of the
23 deformity is a biomechanical phenomenon [36]. It is important to characterize the lateral
24 distribution of bone density within scoliotic vertebral bodies because density variations represent
25 an adaptive response to asymmetrical loading, affect the compressive stiffness of vertebral bodies,

1 and are the key determinant of pullout resistance for implants used in anterior scoliosis surgery.
2 With these considerations in mind, the aim of this study was to quantify lateral bone density
3 variations throughout the thoracolumbar spine in a group of AIS patients, and to explore how the
4 lateral bone density profile is affected by patient characteristics, vertebral level and scoliosis curve
5 severity.

6
7 The results of this study show a marked convex/concave asymmetry in bone density for vertebral
8 levels at or near the apex of the scoliotic curve. At the apical vertebra of the deformity, the mean
9 bone density at the left side (concave) cortical shell was 23.5% higher than for the right (convex)
10 cortical shell. Also at the apex, cancellous bone density along the central 60% of the lateral path
11 from convex to concave increased by 13.8%. The Centre of Mass of the bone density profile at the
12 thoracic curve apex was located 53.8% of the distance along the lateral path, indicating a nearly
13 4% shift toward the concavity of the deformity. These lateral bone density gradients tapered off
14 when moving away from the apical vertebra, so that at the upper and lower vertebrae of the major
15 curve (typically T6 and T12 respectively), bone density was approximately symmetrical about the
16 midpoint of the lateral path.

17
18 Moving into the proximal compensatory curve (upper thoracic levels) however, the trend was
19 reversed, with a 12% decrease in bone density from right to left along the central 60% of the
20 lateral path in the T3 vertebral body, and a 20% drop between right and left cortical shell peak
21 bone densities. These reversals of bone density profile reflect the fact that the proximal
22 compensatory curve is a left thoracic curve, balancing the right thoracic major curve. There were
23 similar reversals in bone density profile for the lumbar vertebrae due to the presence of distal
24 compensatory curves, but these were of lesser magnitude than the lateral bone density gradients in
25 the proximal and main thoracic curves.

1
2 As indicated by Figures 5, 6 and 7, there are significant level-to-level variations in bone density in
3 scoliotic spines. In particular, the mean cancellous bone density (MCP) in Figure 5 is much higher
4 in the thoracic spine than the lumbar spine (where bone density is usually assessed), and bone
5 density at the apex of the major (~T9) and proximal (~T2) scoliotic curves tends to be higher than
6 at neighboring levels. Lateral bone density gradients (GCP) in Figure 6 are clearly affected by the
7 scoliotic curvature, with higher bone density gradients near the apices of the major and
8 compensatory scoliotic curves. Similarly for the Centre of Mass (COM) locations in Figure 7,
9 bone migrates toward the concavity of the apex.

10
11 The multi-linear regressions in Table 4 suggest that the right cortical shell peak bone density is
12 significantly correlated with skeletal maturity, with each Risser increment corresponding to an
13 increase in mineral equivalent bone density of approx. $4 \text{ mg.cm}^{-3} \text{ Ca}$ (between 4-5%). This
14 relationship was statistically significant for 8 of the 17 thoracolumbar vertebrae at the right edge
15 of the lateral path, and for 5 of the 17 vertebrae at the left edge, however there did not appear to be
16 any clear pattern as to which vertebrae had significant correlations. The other regression
17 parameters of note are the statistically significant relationships between patient height, weight and
18 BMI, and GCP (the gradient of cancellous bone density along the central 60% of the lateral path).
19 It appears that while mean cancellous bone density (MCP) is not affected by the independent
20 variables tested, density gradient (GCP) is positively correlated with weight, and negatively
21 correlated with height and BMI. At the apical vertebra, a unit decrease in BMI corresponds to an
22 $18 \text{ mg.cm}^{-3} \text{ Ca}$ (almost 100%) increase in bone density gradient.

23
24 As mentioned in the introduction, the only previous studies of bone density distribution in AIS of
25 which we are aware are those of Périé *et al* [30-32], who reported a coronal plane ‘mechanical

1 migration' of 0.54mm toward the concavity of the scoliotic curve in the lumbar apical vertebrae of
2 11 scoliosis patients. Although our Centre of Mass (COM) is expressed as a percentage of lateral
3 vertebral width, it is essentially the same measure as Périé's mechanical migration. Figure 7 shows
4 that our shift in bone density distribution toward the concavity of the scoliotic curve is about 2%
5 of vertebral width for the lumbar curve apex (generally L3 in our patient group). For a typical
6 vertebral width of 40mm, a 2% shift corresponds to 0.8mm. This value is slightly larger than
7 Périé's shift of 0.54mm, but this may be accounted for by the greater severity of scoliosis in our
8 cohort (mean Cobb angle in our study was 50.5°, compared to 22° in [31]). At the apex of the
9 thoracic major curve (generally T9 in our patient group, but thoracic levels were not measured in
10 Périé's study), our Centre of Mass shift was 3.8%, almost double that of the lumbar curve apex.
11

12 From a bone adaptation perspective, these results suggest that the axial loading on the scoliotic
13 spine is markedly asymmetric. If we make the assumption (based on the Hueter-Volkman
14 principle) that bone density is proportional to compressive stress, then the left/right asymmetry in
15 bone density found in this study suggests that the apical vertebra is subjected to 20-25% more
16 compressive stress on the concave side than on the convex side (based on cortical shell peak bone
17 densities LSP and RSP). The difference in compressive stress acting on the cancellous core
18 between concave and convex sides is somewhat less (~15%, based on the gradient of the central
19 path GCP), but this lesser figure is expected since the region on which the GCP calculation is
20 based only extends 60% of the way to the lateral edge of the vertebra in each direction. These
21 postulated stress asymmetries would tend to move the resultant compressive force vector toward
22 the concavity of the scoliotic curve, a direction consistent with the calculations of Stokes [37],
23 who used a 2D coronal plane simulation to predict the 'vicious cycle' of scoliosis progression
24 under asymmetrical loading. Stokes stated that concave to convex differences in compressive
25 stress in the simulations were in the order of $\pm 10\%$ of the average stress, which implies a

1 difference of 20% between concave and convex sides, in close agreement with our estimated stress
2 asymmetry based on the lateral bone density distribution.

3
4 As well as indicating stress asymmetry, the bone density variations in this study have implications
5 for vertebral stiffness, and for the fixation strength of scoliosis surgery implants. If bone elastic
6 modulus is linearly proportional to bone density as assumed in [37], then the axial stiffness of
7 scoliotic vertebrae will likely vary by a similar amount (20-25%) as the bone density variation
8 from convex to concave sides of the vertebral body. This statement should be treated with caution
9 however, because we only measured bone density at mid-height through the vertebral body,
10 whereas axial stiffness will also depend on the axial distribution of bone density. With regard to
11 anterior implant fixation during scoliosis surgery, the results of this study imply that screws
12 inserted on the convex side of the main thoracic curve will be entering (relatively) lower density
13 bone, so the majority of the fixation strength would be expected to come from the bone adjacent to
14 the distal end of the screw. Given the different in peak density between convex and concave
15 cortical shells, bi-cortical fixation may be of some importance in obtaining a secure implant-bone
16 connection. The question of whether the vertebral bone density distribution correlates with
17 surgical outcomes (e.g. risk of screw pullout or correction achieved) will be the subject of a future
18 investigation.

19
20 Several previous authors have observed lateral migration of bone mass toward the concavity of the
21 deformity in scoliotic spines, but to our knowledge this is the first detailed, quantitative
22 investigation of lateral bone density profiles in adolescent scoliosis. One strength of this study is
23 the use of CT scans, allowing quantitative assessment of mineral equivalent bone densities along a
24 clearly defined 3D path, which is not possible with magnetic resonance images or plain
25 radiographs. Also, the patient group was a reasonably large and homogeneous group (53 female

1 patients with right-sided idiopathic scoliosis and Lenke 1 type curves), representative of the most
2 commonly occurring gender and deformity type among idiopathic scoliosis patients. Further, since
3 the CT scans were originally performed for surgical planning purposes, the deformities were
4 moderate to severe in magnitude (range of Cobb angles 38° to 68°), allowing an investigation of
5 bone density for anatomically and functionally significant deformities.

6

7 A weakness of this study is the fact that we did not have access to comparative CT data for a non-
8 scoliotic control group. Also, the low dose CT protocol used often suffers from image noise at T1
9 due to x-ray beam attenuation by the scapula and ribs. This is noticeable in the greater spread
10 between 10th and 90th percentiles for T1 profile (compared to the other vertebral levels) in Figure
11 4. A third shortcoming of the study is the potential for volume averaging effects to affect cortical
12 shell peak bone density values, since the thickness of the cortical shell is generally less than 1mm,
13 and this is of the same order as the pixel size in the reconstructed images. For this reason, cortical
14 shell peak values LSP and RSP for individual patients are not reliable, and only descriptive
15 statistics based on the entire group of 53 patients were reported in this study.

16

17 This study has presented an original investigation into lateral bone density profiles in idiopathic
18 scoliosis. There are significant concave to convex side asymmetries (up to 23% for cortical shell
19 peak bone density, 14% for cancellous core bone density, and 4% for Centre of Mass offset) in
20 scoliotic vertebrae, particularly near the apex levels of the major and compensatory scoliotic
21 curves.

22

23

References

- 1
- 2
- 3 [1] Landry C, Labelle H, Danserau J, Liberge J, Asher M, De Guise J, 1998. Morphometric
4 characteristics of the scoliotic spine. *Ann Chir.* 52:784-90.
- 5
- 6 [2] Aubin CE, Dansereau J, Petit Y, Parent F, de Guise JA, Labelle H, 1998. Three-dimensional
7 measurement of wedged scoliotic vertebrae and intervertebral disks. *Eur Spine J.* 1998;7(1):59-65.
- 8
- 9 [3] Stokes IA, Aronsson DD, 2001. Disc and vertebral wedging in patients with progressive
10 scoliosis. *J Spinal Disord.* 14:317-22.
- 11
- 12 [4] Parent S, Labelle H, Skalli W, Latimer B, de Guise J, 2002. Morphometric analysis of
13 anatomic scoliotic specimens. *Spine* Nov 1;27(21):2305-11.
- 14
- 15 [5] Liljenqvist UR, Allkemper T, Hackenberg L, Link TM, Steinbeck J, Halm HF, 2002. Analysis
16 of vertebral morphology in idiopathic scoliosis with use of magnetic resonance imaging and
17 multiplanar reconstruction. *J Bone Joint Surg Am* 84-A:359-68.
- 18
- 19 [6] Majcher P, Fatyga M, Krupski W, Tatar M, 2003. The radiological imaging of the vertebral
20 body and intervertebral discs wedging in idiopathic, right-side, thoracic scoliosis as a prognostic
21 factor of the angular progression of spine curve. *Ortop Traumatol Rehabil.* 5:659-65.
- 22
- 23 [7] Parent S, Labelle H, Skalli W, de Guise J, 2004. Vertebral wedging characteristic changes in
24 scoliotic spines. *Spine* 29:E455-62.
- 25

- 1 [8] Modi HN, Suh SW, Song HR, Yang JH, Kim HJ, Modi CH, 2008. Differential wedging of
2 vertebral body and intervertebral disc in thoracic and lumbar spine in adolescent idiopathic
3 scoliosis - A cross sectional study in 150 patients. *Scoliosis* 3;3:11.
4
- 5 [9] Masharawi Y, Salame K, Mirovsky Y, Peleg S, Dar G, Steinberg N, Hershkovitz I, 2008.
6 Vertebral body shape variation in the thoracic and lumbar spine: characterization of its asymmetry
7 and wedging. *Clin Anat* 21:46-54.
8
- 9 [10] Rajwani T, Bagnall KM, Lambert R, Videman T, Kautz J, Moreau M, Mahood J, Raso VJ,
10 Bhargava R, 2004. Using magnetic resonance imaging to characterize pedicle asymmetry in both
11 normal patients and patients with adolescent idiopathic scoliosis. *Spine* 29:E145-52.
12
- 13 [11] Chu WC, Yeung HY, Chau WW, Lam WW, Ng BK, Lam TP, Lee KM, Cheng JC, 2006.
14 Changes in vertebral neural arch morphometry and functional tethering of spinal cord in
15 adolescent idiopathic scoliosis--study with multi-planar reformat magnetic resonance imaging.
16 *Stud Health Tech Inform* 123:27-33.
17
- 18 [12] Huynh AM, Aubin CE, Rajwani T, Bagnall KM, Villemure I, 2007. Pedicle growth
19 asymmetry as a cause of adolescent idiopathic scoliosis: a biomechanical study. *Eur Spine J*
20 16:523-9.
21
- 22 [13] Taylor JR. Scoliosis and growth, patterns of asymmetry in normal vertebral growth, 1983.
23 *Acta Orthop Scand* 54:596-602.
24

- 1 [14] Xiong B, Sevastik B, Sevastik J, Hedlund R, Suliman I, Kristjansson S, 1995. Horizontal
2 plane morphometry of normal and scoliotic vertebrae. A methodological study. *Eur Spine J* 4:6-
3 10.
4
- 5 [15] Sevastik B, Xiong B, Sevastik J, Hedlund R, Suliman I, 1995. Vertebral rotation and pedicle
6 length asymmetry in the normal adult spine. *Eur Spine J* 4:95-7.
7
- 8 [16] Xiong B, Sevastik J, Hedlund R, Sevastik B, 1994. Sagittal configuration of the spine and
9 growth of the posterior elements in early scoliosis. *J Orthop Res* 12:113-8.
10
- 11 [17] Kotwicki T, Napiontek M, 2008. Intravertebral deformation in idiopathic scoliosis: a
12 transverse plane computer tomographic study. *J Pediatr Orthop.* 28:225-9.
13
- 14 [18] Sugimoto Y, Tanaka M, Nakanishi K, Misawa H, Takigawa T, Ozaki T, 2007. Predicting
15 intraoperative vertebral rotation in patients with scoliosis using posterior elements as anatomical
16 landmarks. *Spine* 32:E761-3.
17
- 18 [19] Kotwicki T, Napiontek M, 2002. Torsional deformity of apical vertebra in adolescent
19 idiopathic scoliosis. *Stud Health Tech Inform* 88:360-4.
20
- 21 [20] Wever DJ, Veldhuizen AG, Klein JP, Webb PJ, Nijenbanning G, Cool JC, v Horn JR, 1999.
22 A biomechanical analysis of the vertebral and rib deformities in structural scoliosis
23 *Eur Spine J* 8:252-60.
24

- 1 [21] Herzenberg JE, Waanders NA, Closkey RF, Schultz AB, Hensinger RN, 1990. Cobb angle
2 versus spinous process angle in adolescent idiopathic scoliosis. The relationship of the anterior
3 and posterior deformities. *Spine* 15:874-9.
- 4
- 5 [22] Birchall D, Hughes DG, Hindle J, Robinson L, Williamson JB, 1997. Measurement of
6 vertebral rotation in adolescent idiopathic scoliosis using three-dimensional magnetic resonance
7 imaging. *Spine* 22:2403-7.
- 8
- 9 [23] Adam CJ & Askin GN, 2008. Gravity-induced torque and intravertebral rotation in idiopathic
10 scoliosis. *Spine* 33:E30-7.
- 11
- 12 [24] Asnis SE, Ernberg JJ, Bostrum MPG, Wright TM, Harrington RM, Tencer A, Peterson M,
13 1996. Cancellous bone screw thread design and holding power. *J Orthop Trauma* 10: 462-9.
- 14
- 15 [25] Gatehouse SC, Izatt MT, Adam CJ, Harvey JR, Labrom RD, Askin GN, 2007. Perioperative
16 aspects of endoscopic anterior scoliosis surgery: the learning curve for a consecutive series of 100
17 patients. *J Spinal Disord Tech* 20:317-23.
- 18
- 19 [26] Cheng JC, Guo X (1997) Osteopenia in adolescent idiopathic scoliosis. A primary problem or
20 secondary to the spinal deformity? *Spine* 22:1716–1721.
- 21
- 22 [27] Cheng JCY, Qin L, Cheung CSK, Sher AHL, Lee KM, Ng SWE, Guo X, 2000. Generalized
23 low areal and volumetric bone mineral density in adolescent idiopathic scoliosis. *J Bone Miner*
24 *Res* 15:1587-95.

25

- 1 [28] Lee WTK, Cheung CSK, Guo X, Qin L, Lam TP, Ng BKW, Cheng JCY, 2005. Association
2 of osteopenia with curve severity in adolescent idiopathic scoliosis: a study of 919 girls.
3 *Osteoporosis Int* 16:1924-32.
4
- 5 [29] Szalay EA, Bosch P, Schwend RM, Buggie B, Tandberg D, Sherman F, 2008. Adolescents
6 with idiopathic scoliosis are not osteoporotic. *Spine* 33:802-6.
7
- 8 [30] Périé D, Curnier D, Sales De Gauzy J, 2003. Correlation between nucleus zone migration
9 within scoliotic intervertebral discs and mechanical properties distribution within scoliotic
10 vertebrae. *Magnetic Resonance Imaging* 21:949–953.
11
- 12 [31] Périé D, Curnier D, Sales De Gauzy J, Baunin C, Hobartho MC, 2001. Tomodensitometry
13 measurements for in vivo quantification of mechanical properties of scoliotic vertebrae. *Clinical*
14 *Biomechanics* 16:373-9.
15
- 16 [32] Périé D, Hobatho MC, Baunin C, Sales De Gauzy J, 2002. Personalised mechanical
17 properties of scoliotic vertebrae determined in vivo using tomodensitometry. *Comput Methods*
18 *Biomech Biomed Engin* 5:161-5.
19
- 20 [33] Routh RH, Rumancik S, Pathak RD, Burshell AL, Nauman EA, 2005. *Osteoporosis Int*
21 16:1857-63.
22
- 23 [34] Kamimura M, Kinoshita T, Itoh H, Yuzawa Y, Takahashi J, Hirabayashi H, Nakamura I,
24 2002. Preoperative CT examination for accurate and safe anterior spinal instrumentation surgery
25 with endoscopic approach. *J Spinal Disord Tech* 15(1): 47-51.

1
2 [35] Lenke LG, Betz RR, Harms J, Bridswell KH, Clements DH, Lowe TG, Blanke K, 2001.
3 Adolescent idiopathic scoliosis: a new classification to determine extent of spinal arthrodesis. *J*
4 *Bone Joint Surg Am* 83-A:1169-81.
5
6 [36] Roaf R, 1966. The basic anatomy of scoliosis. *J Bone Joint Surg* 48:786–92.
7
8 [37] Stokes IA, 2007. Analysis and simulation of progressive adolescent scoliosis by
9 biomechanical growth modulation. *Eur Spine J* 16:1621-8.
10
11
12

Figures & Captions

1
2
3
4
5
6
7
8
9
10
11
12
13
14
15
16
17
18
19
20
21
22
23
24
25

Figure 1.

Reformatted CT scan of adolescent idiopathic scoliosis patient showing the (right thoracic) major curve, the proximal and distal compensatory curves, the major curve Cobb angle measurement, and the apical vertebra. The red lines indicate the reslice planes through the mid-height of each vertebral body which were used to define the lateral paths for bone density assessment (only four reslice planes are shown for clarity).

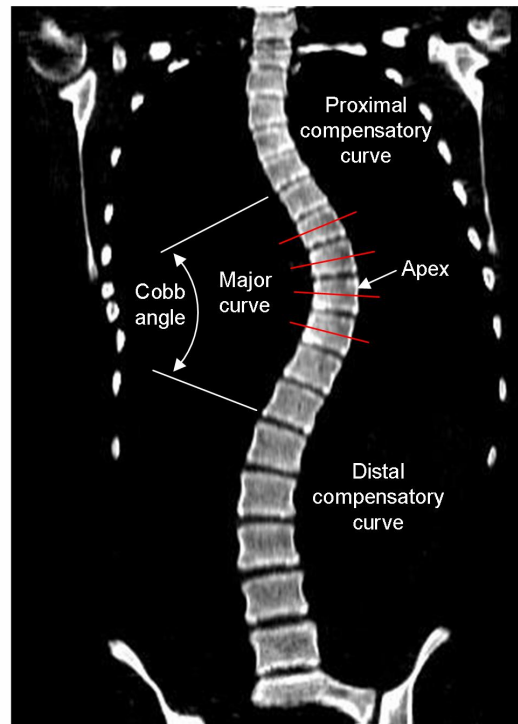
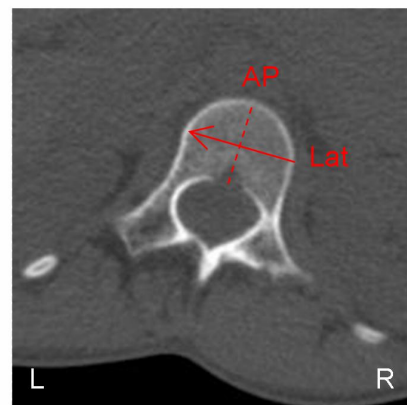


Figure 2.

View of a reslice plane showing the definition of the AP and lateral paths. The lateral path is drawn perpendicular to the AP line through the maximum width of the vertebral body. The arrow on the lateral path indicates the right → left direction for normalized path distance.



1
2
3
4
5
6
7
8
9
10
11
12
13
14
15
16
17
18
19
20
21
22
23
24
25

Figure 3.

Schematic bone density profile along the lateral path, showing the interpretation of each of the bone density profile parameters (RSP, LSP, MCP, GCP, COM).

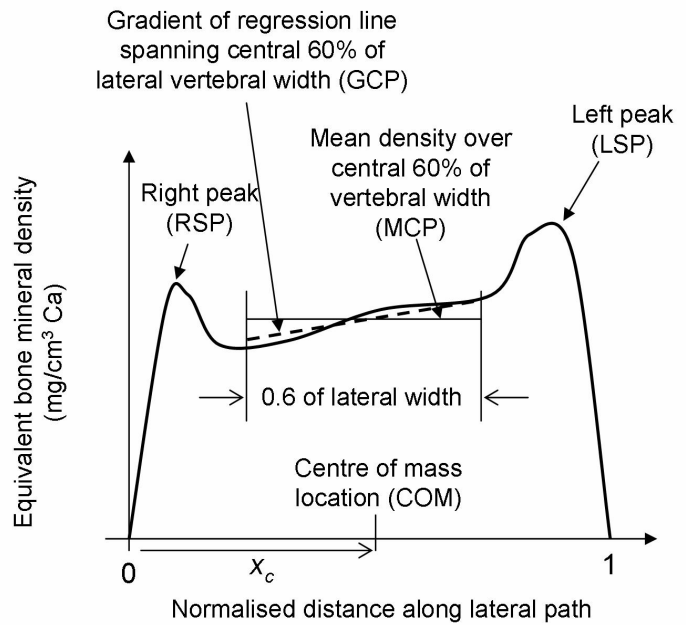
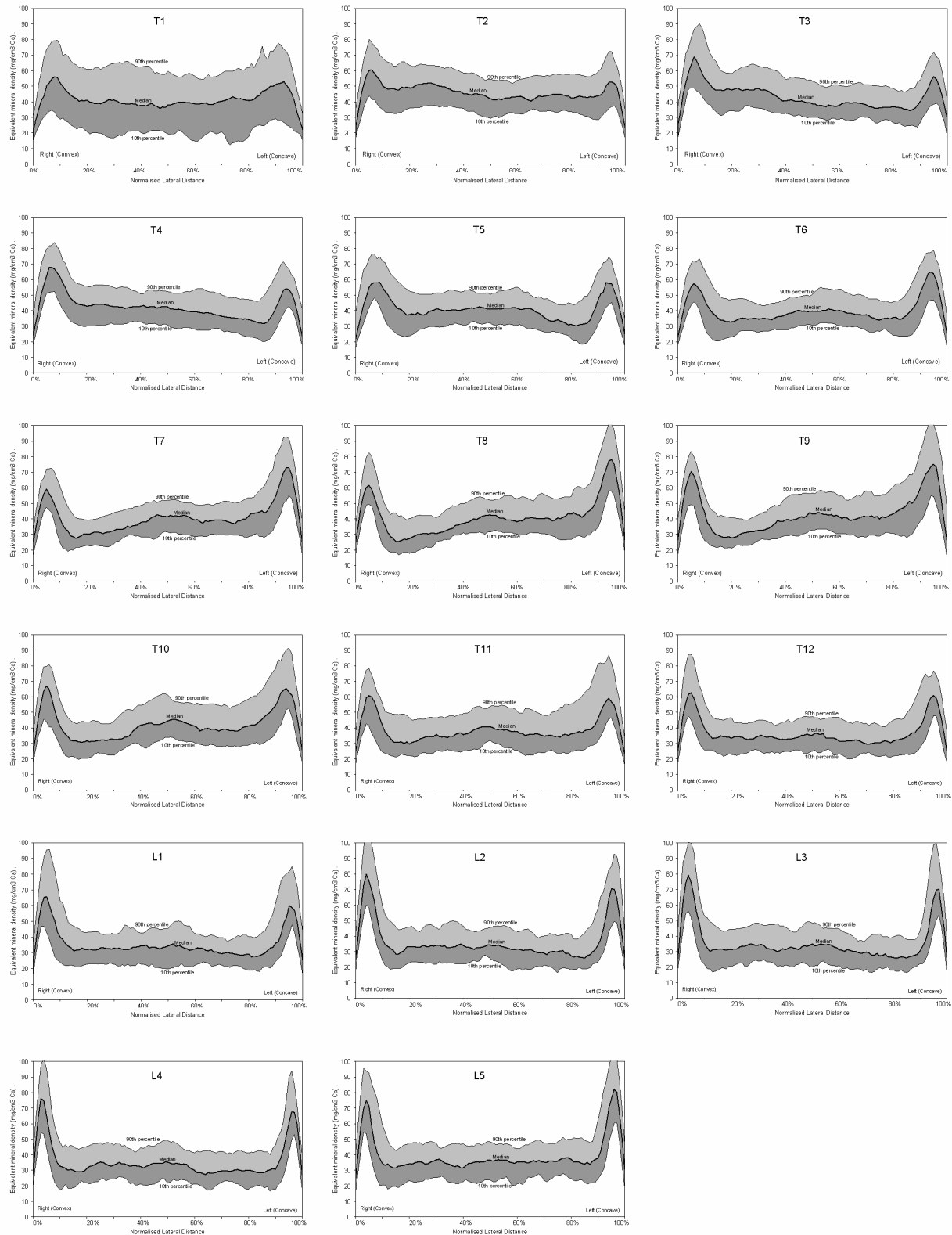


Figure 4.

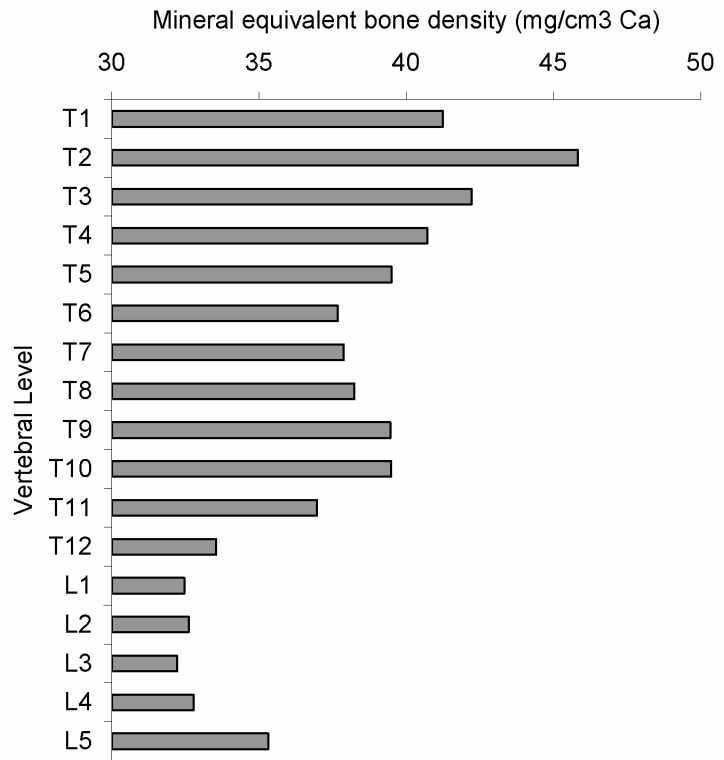
See next page

1 **Figure 4.**

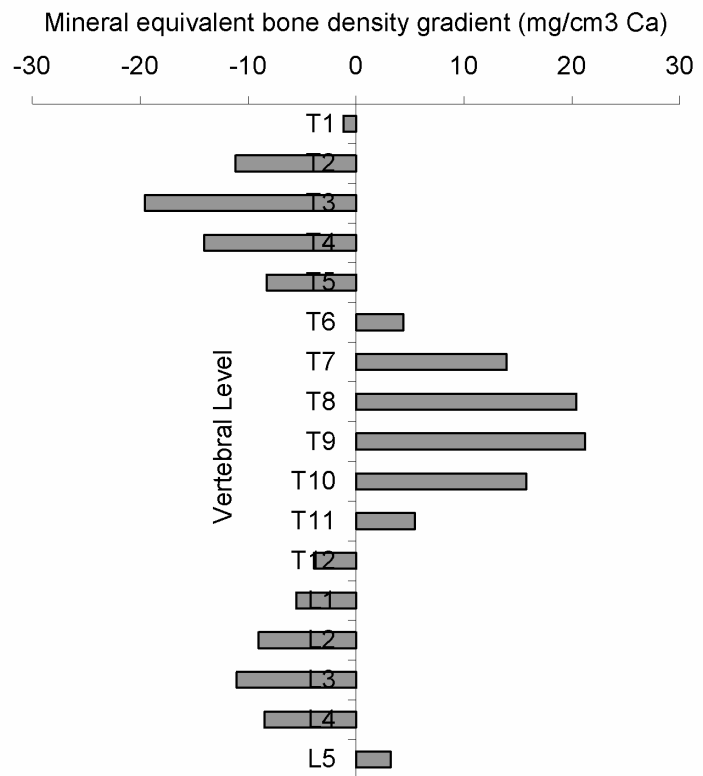
- 2 10th, 50th (median) and 90th percentile bone mineral density profiles along the lateral path for each
- 3 vertebral level from T1 to L5 for the entire patient cohort.



1 **Figure 5.**
 2 Mean bone density along the
 3 central 60% of the lateral path
 4 (MCP, in $\text{mg}\cdot\text{cm}^{-3}$ Ca) versus
 5 vertebral level for the entire
 6 patient cohort.



15 **Figure 6.**
 16 Gradient of bone density along the
 17 central 60% of the Lateral path
 18 (GCP, in $\text{mg}\cdot\text{cm}^{-3}$ Ca) versus
 19 vertebral level for the entire patient
 20 cohort.



1 **Figure 7.**
2 Centre of Mass location
3 along the lateral path
4 (COM, normalized distance
5 in %) versus vertebral level
6 for the entire patient cohort.
7
8
9
10
11

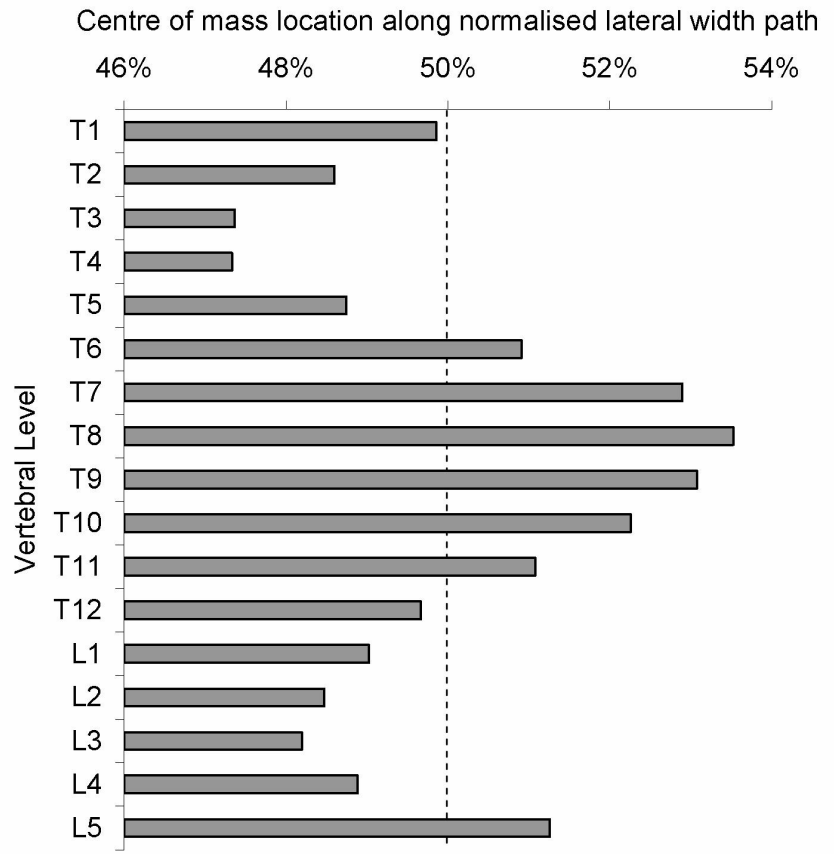


Table 1. Patient group demographics

Number of patients	53 (all female)
Mean age (\pm sd)	15.6 \pm 4.5 yrs
Mean height (\pm sd)	161 \pm 7 cm
Mean weight (\pm sd)	52.5 \pm 10.2 kg
Mean BMI (\pm sd)	20.2 \pm 3.3 kg.m ⁻²
Major curve type	Right thoracic (Lenke 1)
Mean major Cobb (\pm sd)	50.5 \pm 6.9°

Table 2. Lateral bone density profile parameters versus vertebral level. All densities are mineral equivalent bone density ($\text{mg}\cdot\text{cm}^{-3}\text{ Ca}$)

	T1	T2	T3	T4	T5	T6	T7	T8	T9	T10	T11	T12	L1	L2	L3	L4	L5
RSP	Max bone density at convex peak																
Mean	63	65	71	71.0	65	61	62	66	71	68	63	68	73	84	83	79	80
St Dev	16	13	15	12.3	12	12	11	12	13	14	13	16	20	18	17	18	18
Min	37	39	37	52.4	42	37	38	48	37	40	34	38	42	54	52	45	45
Max	103	100	99	98.8	96	100	91	95	96	99	90	116	140	122	132	120	125
Median	64	66	70	71.6	65	59	61	65	73	69	64	68	71	81	83	77	79
LSP	Max bone density at concave peak																
Mean	65	58	59	58.5	60	67	76	81	82	73	67	66	69	75	75	72	89
St Dev	16	13	12	12.1	12	12	15	17	20	8	16	11	16	18	18	16	20
Min	30	40	37	38.6	34	42	49	47	44	24	39	39	44	47	44	33	55
Max	103	94	92	87.8	88	95	116	119	125	59	99	85	121	125	122	115	153
Median	63	57	60	57.4	60	65	76	79	79	38	65	66	70	74	74	71	88
MCP	Mean bone density along central 0.6 of lateral path																
Mean	41	46	42	40.7	40	38	38	38	39	39	37	34	32	33	32	33	35
St Dev	14	8	8	7.4	7	7	7	7	7	8	8	7	7	7	8	7	8
Min	14	28	26	27.7	24	24	26	24	26	24	23	22	20	21	18	21	19
Max	68	61	61	56.0	55	53	52	57	56	59	55	48	49	52	50	49	49
Median	41	46	40	40.6	39	37	37	38	37	38	36	33	32	32	32	31	35
GCP	Slope of regression line along central 0.6 of lateral path																
Mean	-1	-11	-20	-14.1	-8	4	14	20	21	16	5	-4	-6	-9	-11	-8	3
St Dev	20	15	14	16.9	13	11	15	13	17	14	14	11	11	12	12	11	11
Min	-51	-44	-74	-46.3	-32	-19	-15	-3	-6	-22	-25	-28	-30	-37	-43	-33	-38
Max	41	22	10	37.6	20	33	48	49	72	47	48	30	16	20	14	20	23
Median	0	-10	-18	-17.2	-9	4	12	24	21	15	5	-4	-5	-8	-8	-6	1
COM	Centre of mass (normalized distance along lateral path)																
Mean	0.499	0.486	0.474	0.473	0.487	0.509	0.529	0.535	0.531	0.523	0.511	0.497	0.490	0.485	0.482	0.489	0.513
St Dev	0.026	0.017	0.019	0.022	0.023	0.021	0.021	0.021	0.020	0.016	0.018	0.022	0.025	0.022	0.022	0.021	0.020
Min	0.442	0.446	0.436	0.430	0.446	0.470	0.482	0.487	0.481	0.483	0.446	0.445	0.437	0.433	0.389	0.411	0.463
Max	0.558	0.517	0.540	0.533	0.551	0.564	0.588	0.580	0.582	0.553	0.546	0.542	0.541	0.535	0.530	0.534	0.567
Median	0.500	0.487	0.473	0.471	0.489	0.511	0.530	0.536	0.533	0.524	0.512	0.498	0.493	0.483	0.484	0.493	0.511

Table 3. Lateral bone density profile measures relative to the coronal apex (A) of the scoliotic curve. Negatives are superior to apex, positive levels inferior. All densities are mineral equivalent bone density ($\text{mg}\cdot\text{cm}^{-3}\text{Ca}$)

	A-3	A-2	A-1	A	A+1	A+2	A+3
RSP	Max bone density at convex peak						
Mean	63	60	64	68	70	67	64
St Dev	11	11	12	12	14	13	14
Min	37	42	38	44	42	37	34
Max	89	84	92	95	99	90	96
Median	62	59	63	65	69	69	63
LSP	Max bone density at concave peak						
Mean	62	71	79	84	80	69	67
St Dev	11	13	16	17	20	13	13
Min	42	47	49	50	44	48	46
Max	89	102	116	125	125	102	99
Median	64	72	76	83	77	66	66
MCP	Mean bone density along central 0.6 of lateral path						
Mean	39	38	38	39	39	39	36
St Dev	7	7	7	7	8	9	7
Min	24	24	26	26	23	25	23
Max	55	52	57	56	59	56	53
Median	39	37	37	38	38	37	35
GCP	Slope of regression line along central 0.6 of lateral path						
Mean	-5	7	16	23	19	14	4
St Dev	13	12	13	15	17	14	12
Min	-29	-15	-3	-10	-22	-25	-28
Max	33	48	49	57	72	48	36
Median	-4	5	13	26	20	13	4
COM	Centre of mass (normalized distance along lateral path)						
Mean	0.494	0.516	0.532	0.538	0.529	0.518	0.508
St Dev	0.019	0.018	0.020	0.017	0.019	0.017	0.020
Min	0.455	0.474	0.482	0.505	0.491	0.474	0.445
Max	0.564	0.560	0.588	0.582	0.581	0.549	0.540
Median	0.494	0.518	0.531	0.536	0.531	0.518	0.511

Table 4. Statistically significant ($P < 0.05$) terms in the multi-linear regressions. Five separate regressions were performed at each vertebral level, for dependent variables RSP, LSP, MCP, GCP, COM. The independent variables in each case were; age, height, weight, BMI, major Cobb angle, Risser sign, months since Menarche, upper and lower vertebral levels of the major curve. Numbers in brackets indicate the corresponding coefficient in the regression equation.

Level	RSP	LSP	MCP	GCP	COM
T1		Cobb (-0.80)			
T2			Risser (2.098)		
T3	Age (-1.38) Risser (5.16)	Risser (3.27)	Age (-0.72) Risser (2.51)	Height (5.23) Weight (-7.84) BMI (20.37)	Age (0.002)
T4	Risser (3.67)			Cobb (-0.82) Lower (9.78)	Age (-0.002)
T5		Apex (-8.22) Lower (6.30)			
T6	Risser (4.51)			Height (-4.18) Weight (7.12) BMI (-18.38)	Height (-0.006) Weight (0.01) BMI (-0.026) Risser (-0.005)
T7	Risser (3.32)			Cobb (.561)	Risser (-0.005) Cobb (+0.001)
T8	Risser (3.08)	Risser (4.49)		Height (-3.55) BMI (-12.9)	Cobb (0.001)
T9	Risser (3.74) Cobb (0.46)	Risser (4.61)		Upper (14.23)	Menarche (0.00)
T10	Risser (4.32)	Risser (4.02)		Menarche (-0.3)	Age (0.013) Menarche (0.00)
T11	Risser (5.44) Upper (9.26)	Risser (4.68) Lower (7.90)	Risser (2.56)		Lower (0.01)
T12					
L1					Upper (0.02) Apex (-0.025)
L2				Lower (6.37)	
L3	Risser (4.99)	Risser (6.27)	Risser (1.97)	Weight (6.04) BMI (-15.25)	
L4	Lower (9.86)		Risser (2.32) Upper (6.31) Apex (-5.33)	Weight (4.86) BMI (-12.97)	
L5			Cobb (-0.355)		
Vertebral level relative to apical vertebra (A)					
A-3				Weight (5.79) BMI (-14.76)	
A-2	Risser (3.18)			Cobb (0.50)	
A-1	Risser (3.52)			Risser (-2.92) Upper (7.95)	
A				Height (-5.30) Weight (7.43) BMI (-18.84)	Height (-0.006) Weight (0.008) BMI (-0.02)
A+1	Age (-1.02) Risser (5.47)	Risser (5.13)		Risser (4.49) Menarche (-0.33) Upper (11.04) Apex (-14.43)	Menarche (0.00)
A+2	Risser (4.66)	Risser (4.97)	Risser (2.26)		
A+3			Risser (1.98)	Apex (-11.5)	

Appendix 1. Summary of patient details

Patient #	Age (yr)	Height (cm)	Weight (kg)	BMI (kg.m ⁻²)	Risser	Menarche (months)	Cobb (°)	Major curve levels		
								Upper	Apex	Lower
1	13.3	153	45	19.2	1	14	58	T6	T9	T12
2	27.8	151	45	19.7	5	60	45	T6	T9	T12
3	13.1	154	42	17.7	0	0	60	T5	T9	T12
4	14.7	157	39.5	16.0	1	0	52	T5	T8/9	T12
5	12.7	157	53	21.5	3	44	47	T4	T8	T12
6	16.5	160	48	18.8	5	36	51	T5	T9	T12
7	13.6	163	49.7	18.7	4	7	50	T4	T8	T12
8	13.3	158	42	16.8	2	38	54	T5	T9	T11
9	15.4	164	49	18.2	4	19	42	T5	T8/9	T12
10	14.1	165	65	23.9	4	25	44	T5	T8/9	T12
11	15.5	153.5	44	18.7	4	34	48	T5	T8	T11
12	11.2	156	46.7	19.2	0	0	35	T6	T8/9	T11
13	13.2	161	60.9	23.5	3	32	48	T6	T9	T12
14	14.6	158	44.8	17.9	0	5	42	T5	T7/8	T10
15	13.6	158	42	16.8	0	9	52	T6	T9	T12
16	18.1	167.5	52.5	18.7	5	44	56	T5	T8	T12
17	22.4	175	70.8	23.1	5	60	52	T6	T9	T12
18	16.2	164.5	63	23.3	4	32	42	T5	T7	T10
19	13.3	157	41	16.6	0	7	58	T5	T8	T11
20	21.2	163	49	18.4	5	60	51	T6	T10/11	L2
21	14.5	159	47.6	18.8	5	0	60	T5	T8/9	T12
22	16.5	172	65.5	22.1	4	48	52	T6	T8	T12
23	12.1	148	33.6	15.3	0	0	59	T5	T8	T12
24	12.2	156	45	18.5	0	0	64	T5	T9	T13
25	13.8	159	51	20.2	4	10	58	T6	T9	T12
26	17.2	169	62.6	21.9	4	41	43	T5	T8	T10
27	11.2	139.5	34	17.5	0	0	45	T4	T7/8	T12
28	15.1	169.5	48.7	17.0	0	5	50	T5	T8/9	T12
29	15.4	162	60	22.9	3	34	68	T5	T8	T11
30	13.8	164	51.8	19.3	3	7	45	T6	T9	T12
31	16.5	164	54.6	20.3	3	29	54	T5	T8/9	T12
32	12	146	54.7	25.7	0	0	43	T6	T9	L1
33	15.2	173	58.9	19.7	4	29	48	T5	T8	T11
34	13.5	162	51.3	19.5	0	5	55	T5	T8/9	T12
35	14	164	49	18.2	0	0	66	T6	T9	T11
36	16.5	162	52.5	20.0	5	60	48	T6	T11	L1
37	13.3	153	49.4	21.1	1	9	58	T6	T9	T12
38	13.5	169	66	23.1	4	19	54	T5	T8	T10
39	17.4	167	50	17.9	5	34	53	T5	T9	L1
40	17.6	166.5	47.5	17.1	4	23	38	T6	T10	L1
41	41.2	162	58	22.1	5	60	48	T6	T9	T12
42	14.3	158	67	26.8	3	0	46	T5	T8	T12
43	15.4	163	52	19.6	4	60	48	T4	T7	T11
44	13.9	150	42	18.7	0	0	48	T5	T8	T11
45	15.4	160.8	59.6	23.1	5	46	44	T5	T8	T11
46	14.7	156	45.5	18.7	4	18	48	T5	T9/10	L1
47	14.5	167	59.6	21.4	4	20	50	T5	T8/9	T12
48	12.7	159.5	42.9	16.9	0	0	56	T5	T8/9	T12

49	14.9	174.5	62	20.4	4	0	55	T5	T8	T11
50	16.6	163	46.3	17.4		29	52	T5	T8/9	T11
51	14.8	161	84.7	32.7	4	0	43	T4	T7	T11
52	14.3	159	75.7	29.9	2	25	47	T6	T8/9	T13
53	18.2	172	61.7	20.9	5	49	42	T5	T7/8	T10
